N93-26189

# Precision of the Calibration of the AXAF Engineering Test Article (VETA) Mirrors.

D.A. Schwartz, G. Chartas, J.P. Hughes, E.M. Kellogg, and P. Zhao
Smithsonian Astrophysical Observatory

## ABSTRACT

Measurements of the VETA encircled energies have been performed at 5 energies within 16 radii ranging from 0.05 to 200 arcseconds. We report here on the analysis of the accuracy of those measurements. A common "error tree" structure applies, and we present representative numbers for the larger terms. At 0.277, 1.5, and 2.07 keV, and for radii of 3 arcsec and larger, our measurements have estimated 1 sigma errors of 0.6 to 1.5 percent. Effects of measurement statistics and of the VETA test mount limit the accuracy at smaller angles, and modulation by the counter window support structure together with the imperfect position repeatability limit the accuracy for the 0.93 and 2.3 keV energies. We expect to mitigate these limitations when calibrating the complete AXAF flight mirror assembly.

## 1. INTRODUCTION: CALIBRATION OF AXAF

The Advanced X-ray Astrophysics Facility (AXAF) will be a long-lived international observatory for performing high resolution imaging and spectroscopic studies in the 0.1 to 10 keV range. The scientific objectives of AXAF are to investigate the nature of celestial objects, the physics of fundamental processes in the universe, and the history and evolution of the universe. To fully exploit the information obtained requires that we know the response of the X-rays mirrors to a calibration accuracy of order 1%.

We have been investigating techniques for calibrating the flight mirrors in conjunction with previous measurements proving the technology of mirror fabrication. We have previously reported results from measurements of a Technology Mirror Assembly (TMA; Schwartz et al. 1986; VanSpeybroeck et al. 1986; Wyman et al. 1986) and of an improved version of this assembly designated TMA-II, (VanSpeybroeck et al. 1989). The Verification Engineering Test Article (VETA) consisted of the outermost pair of the nested set of AXAF mirrors, comprising the actual flight mirror. Previous results have been reported in Kellogg et al (1991b), in internal SAO reports (Brissenden et al. 1991; 1992), and appear in several papers in this volume. The present paper addresses X-ray measurements of the VETA from the point of view of how accurate a calibration was performed.

Our objective for the VETA calibration was 5% accuracy for the effective area and 2% accuracy for the encircled energy. These were unusual and ambitious goals, which were largely achieved. This requirement forced much attention to details, of which some were unusual and unanticipated (cf., Chartas et al. 1992; Zhao et al. 1992a,b).

The next section discusses the philosophy and objectives of calibration in more detail. In general, the error from photon counting statistics can be made less than 1% since it is usually feasible to acquire more than $10^4$ counts, so that ability to understand the systematic effects determines the final precision. Section 3 presents the principles of the calibration measurements. Our key technique is to measure the ratio of counts in nominally identical detectors, so that many effects, (e.g., variability of the X-ray generator, dead time in the common electronics), cancel to first order. Section 4 presents our detailed analysis of how accurate are the VETA calibration measurements. Papers in this volume by Hughes et al. (1992) and Kellogg et al. (1992) address how well we can use this information to deduce the true properties of the VETA.

## 2. CALIBRATION OBJECTIVES

To understand the rationale of the calibration program, we must clearly define the purposes of calibration. In simplest form, a "calibration" is a measurement that can stand alone to provide definitive numerical conversion of on-orbit data into physical quantities. An approximation to this situation might be the conversion of a counting rate measured in a ten arcsec circle in the focal plane at some off-axis angle, into a broad band flux. The calibration

process might have allowed us to determine a single "average area" number to divide into the measured counting rate.

In X-ray astronomy the flux conversion actually depends on the form of the incident spectrum, and calibration is a much more complex process. It is clearly not possible to reproduce on the ground every possible measurement that could be made on-orbit. That would require sampling the product of all possible energies, times a range in each of two off-axis angles, times a range of focal plane locations, times all possible image sizes of interest. The way the actual flight data is analyzed is by construction of semi-analytical models of the telescope and detectors, and using these models to interpolate and extrapolate continuously to the exact parameter values of any given observation. Thus the second major purpose of a calibration is to verify that the models used are valid.

The third purpose of the calibration is to overdetermine the numerical parameters appearing in the models. This allows determination of best-fit values, error estimates, and allowed ranges of parameters, to any given confidence level.

In cases where the models prove inadequate (e.g., unacceptable fits to the data for any values of the free parameters), the calibration process must provide sufficient data to refine the models. Examples of such refinement might be measuring on a finer grid of data points for interpolation, or replacing the usual assumption of azimuthal symmetry with a detailed functional dependence.

The most general calibration model of a telescope is the point response area:

$$dA(E, \theta, \vartheta, y, z, x, i) \tag{1}$$

where $dA/(dydz)$ is the infinitesimal effective absolute area per unit solid angle in the image plane, to a broad parallel beam of X-rays of energy E, incident at polar angle theta and azimuthal angle phi to the telescope optical axis, and imaged at the angular position y, z in a plane parallel to the on-axis Gaussian focal plane but displaced by a distance x. The two polarization states are indexed by $i$. X-ray reflectivity depends only slightly on the polarization state, and we do not consider this further for the VETA calibration. For the flight mirror, the significance of polarization correction will be investigated.

Operationally, one of the most important functions is the absolute encircled energy area,

$$A_r(E, \theta, \vartheta, x) = \int_0^r dA \; dy \, dz \tag{2}$$

Henceforth we will specialize to the case of the VETA measurements, which were made on-axis, theta=0, phi indeterminate, and in focus, $x = 0$. Dropping $\vartheta$, the effective area is defined as

$$A_{eff}(E) \equiv A_{r=\infty/2}(E, 0, 0). \tag{3}$$

Other important quantities are the dimensionless point response function, $f = dA/A_{eff}$, and the encircled energy fraction $A_r/A_{eff}$.

In this paper we will deal with the encircled energy area, as measured within the available apertures (Podgorski et al. 1992). Effective area will be considered as a limiting case of encircled energy, and treated in more detail by Kellogg et al. (1992).

## 3. PRINCIPLES OF THE VETA CALIBRATION MEASUREMENTS

Figure 1 illustrates the fundamental principle of our calibration. A broad, uniform, parallel beam of X-rays of monochromatic energy E illuminates both the VETA X-ray mirror and a beam normalization detector (BND) immediately adjacent to the VETA. The BND is provided with a large mechanical aperture of a precisely known area, $A_1$. In the focal plane, X-rays which pass through a precisely measured pinhole of angular radius, r, illuminate a focal plane X-ray detector assembly (XDA) which is nominally identical to the BND assembly. These detectors are thin window, gas proportional counters, with a gas flow system to replenish the gas which leaks out through

the windows. Analog pulses resulting from X-ray interactions in the BND and focal plane detectors are processed through nominally identical electronics, and are presented to a common analog to digital converter, the MultiChannel Analyzer (MCA), resulting in numbers $N_1$ and $N_2$ counts, respectively. We then can express the desired encircled energy area as

$$A_r = A_1(N_2/N_1). \tag{4}$$

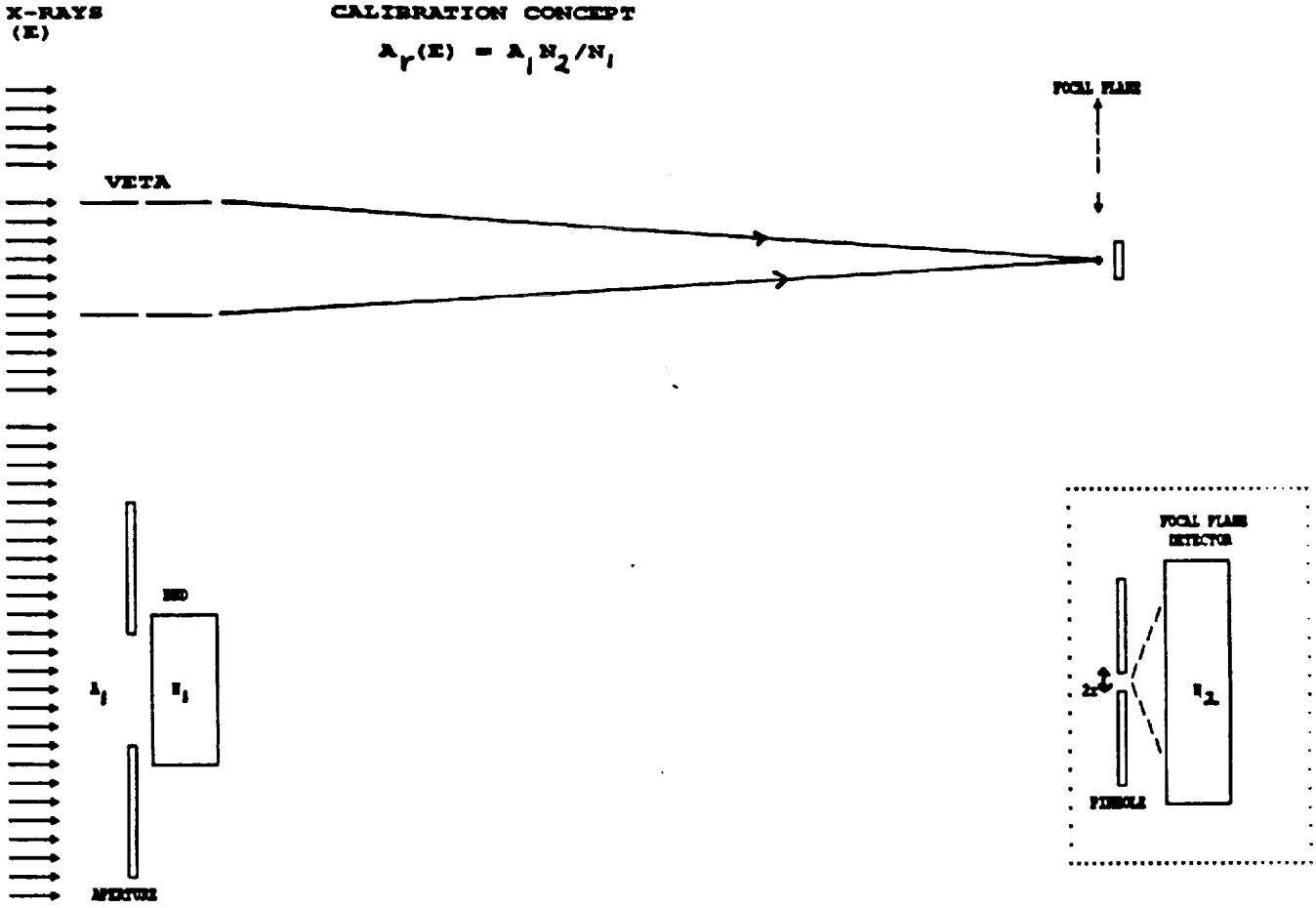


Figure 1. Cartoon of the concept of calibration of an X-ray mirror. The VETA reflects X-rays to the focal plane. The comparison of focal plane counts to counts in an identical detector adjacent to the VETA. provides the required information. The x-ray focus area is enlarged to the lower right. (Figure is not to scale.)

The remaining task of this paper is to construct the error analysis tree, accounting for the extent to which the actual experiment deviates from the above idealization. In this paper we only deal with the errors affecting the accuracy of the measurement. Specifically, the fact that the X-rays are diverging from a source of finite size at finite distance must be considered in converting from our measured parameters to the true VETA model. Since the VETA as such will not be used as a flight instrument, we do not attempt the on-orbit performance estimate in this paper (but cf., Freeman et al. 1992; Hughes et al. 1992;) For the error *analysis* tree presented here we take a data oriented approach, in contrast to the hardware oriented approach presented by Kellogg et al. (1991a) in discussing the error *budget* tree, prior to performing the measurements.

We can see some potential difficulties by reference to Figure 1. We must ask to what extent is the X-ray beam uniform, so that the mean flux over the VETA is identical to that over the $A_1$ aperture. Zhao et al. (1992) discussed the correction due to the fact that the X-rays form a ring on the focal plane detector , whereas they uniformly

illuminate the BND detector. Finally, the X-ray beam consists of broad bremsstrahlung continuum, underlying the idealized emission line spectrum. Chartas et al. (1992) discuss the process of extracting those counts attributable to the line emission.

## 4. ANALYSIS OF THE CALIBRATION ACCURACY

### 4.1 Top Level Encircled Energy Area

Our measurements employed 5 different energies, and 16 different pinhole sizes. Rather than present 80 detailed error analyses leading to the precise uncertainty for each measurement, we want to emphasize the error analysis structure that applies to all measurements. Thus in the discussion below we may quote a range of error values, or nominal values which apply very closely, but not necessarily precisely, to many of the measurements.

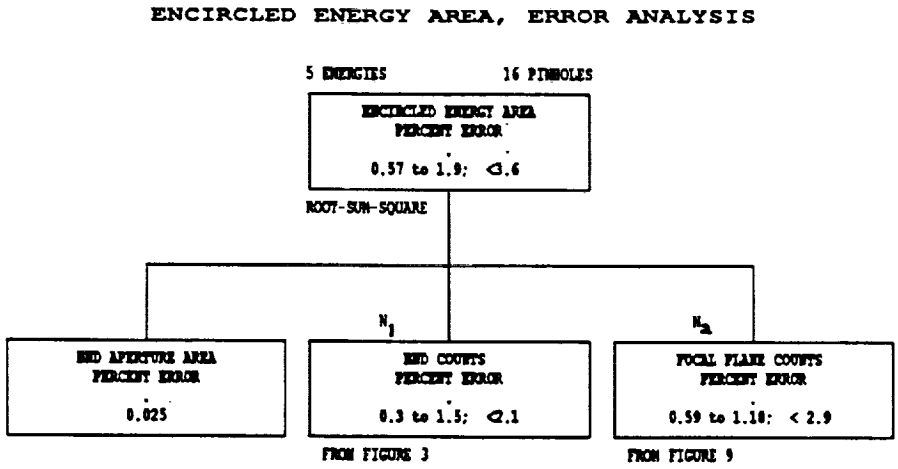


Figure 2. Top level error analysis. The final error in ENCIRCLED ENERGY AREA is shown as the root-sum-square of the three terms on the right hand side of equation (4), where $N_1$ are the BND COUNTS. and $N_2$ are the FOCAL PLANE COUNTS. The error analysis for $N_1$ is shown in figure 3, and the error analysis for $N_2$ is shown in figure 9.

Figure 2 shows the top level of the error analysis tree, based on equation (4). We intend that the three lower terms be combined as a root-sum-squares, to give the net error in the upper box. Thus we attempt to analyze systematic errors which affect both detectors in only one place: as if the BND were correct and the focal plane had a relative error, (or vice versa). The BND aperture is a 20 mm diameter hole, drilled in 1/8th inch aluminum, so that its area is 3.142 $cm^2$. The diameter is measured with a precision Jo block to an estimated accuracy of 0.025%. Effects due to vignetting by the finite thickness of the aperture, and to penetration of the Al plate by X-rays of the energies present in the bremsstrahlung continuum, are estimated at less than $10^{-5}$.

A more accurate description is given by equation (5):

$$A_r(E) = A_1 * (B_1/B_{VETA}) * (N_2'/t_2)/(N_1'/t_1), \quad (5)$$

which considers the ratio of the true counting *rates*, with the live time ratio $(t_1/t_2)$ and the ratio of flux on the BND, $B_1$, to flux on the VETA, $B_{VETA}$, both taken as nominally 1. The primes denote the counts from the X-ray lines,

rather than the total counts in the detectors. These counts, $N_2'$ and $N_1'$, are determined from fits to the proportional counter pulse height spectra, as discussed by Chartas et al. (1992).

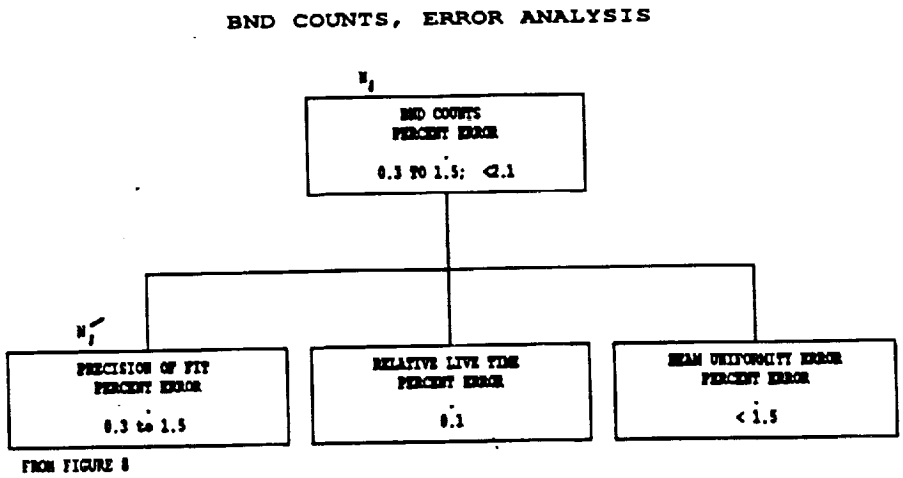


Figure 3. Analysis of the error in the BND COUNTS. The top box represents the net error in $N_1$, and the lower left box the error in determining $N_1'$. The error in $N_1'$ is analyzed in figure 8. Data on the RELATIVE LIVE TIME is shown in figure 4, and data relative to the BEAM UNIFORMITY ERROR is shown in figure 5.

Figure 3 shows the top level error analysis for the idealized BND counts, $N_1$, and Figure 9 for the idealized focal plane counts, $N_2$.

4.2 Error Analysis of the Beam Normalization Detector Counts.

To estimate the live time in each detector chain, we insert a pulse generator of known rate into a portion of the pulse height spectrum where we do not expect significant X-ray counts. Figure 4 plots the dead time determined in this manner for the BND and focal plane counts, separately, as a function of the total counting rate of the MCA. We also plot the dead time measurement which is generated internally by the MCA. We attribute the small differences among these curves, and the fact that they do not have zero intercept, as due to low level noise pulses which do not register as MCA counts, and vary due to different noise levels in different detectors. Our nominal operating point is about 5000 $s^{-1}$, giving a relative error of 0.1%. We analyze this error as applying to the incident flux determined by the BND.

We find no evidence for spatial irregularity of the X-ray beam which would cause the BND to sample a flux different from the VETA. Unfortunately we were not able to do the extensive experimentation necessary to provide stringent limits. Ideally, we would scan one BND in space over the area in front of the VETA, and compare its counting rate to an identical fixed BND detector in order to separate effects of time variability in the X-ray generator. This is planned to be carried out prior to and subsequent to calibration of the actual flight mirrors. At present we have some limited information obtained by scanning the focal plane detector in the broad beam at the focal plane, after the VETA had been removed. Figure 5 shows the ratio of the focal plane (scanning) to BND (fixed) total counts, vs. the position of the focal plane detector over a 600 mm scan in the horizontal direction, with the Al source. If this scan were a fair sample of the VETA aperture, we would quote the maximum allowed rms of the ratio about its mean value, and after root-sum-square subtraction of the counting rate statistics, as the limit to the beam non-uniformity. Instead, to attempt to be more conservative, we quote the total 1.5% change obtained by an eyeball straight line fit to the data. Although this was a horizontal scan, we note that the BND is displaced vertically from the telescope axis. We

may expect that the beam non-uniformity depends on the filter used with each target in the X-ray generator, and thus is specific to each X-ray energy.

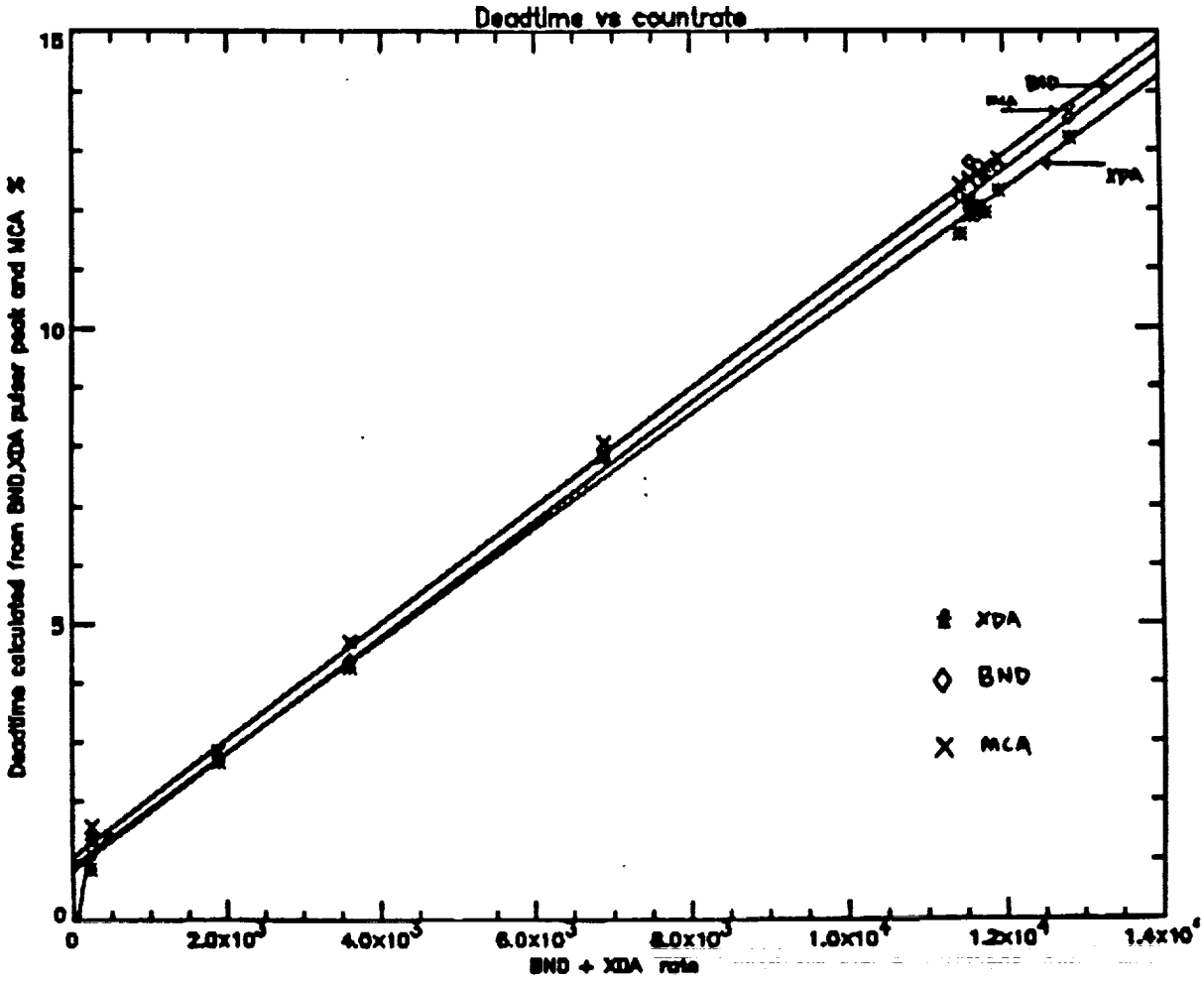


Figure 4. Percent dead time is plotted vs total (i.e., BND plus XDA) counting rate. The dead time is estimated in three different ways: MCA designates the expected dead time as generated by the MCA electronics; BND designates dead time estimated by a pulse generator of known rate through the BND electronics chain, and XDA designates dead time estimated by the same pulse generator through the XDA electronics chain.

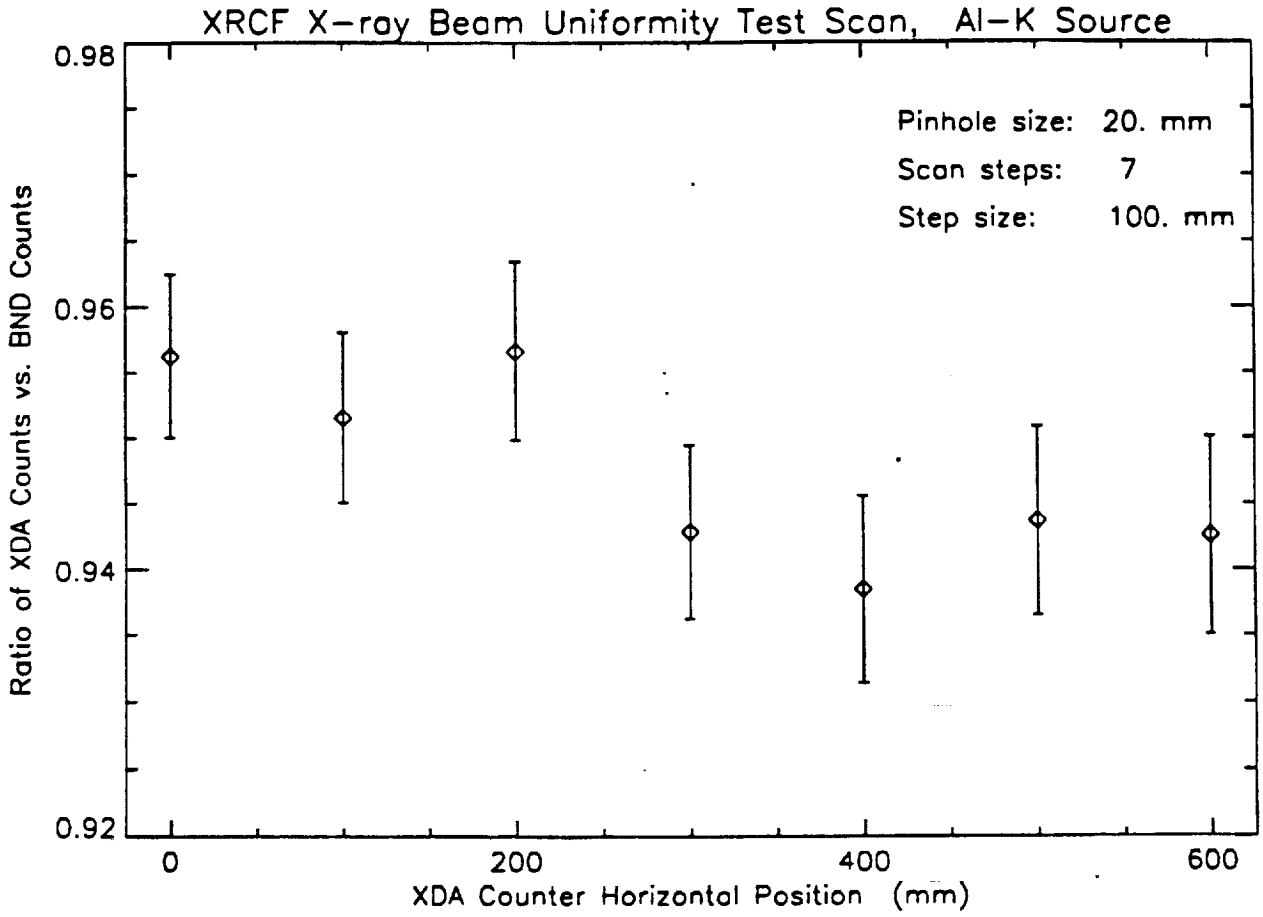


Figure 5. Beam uniformity scan for the Al 1.5 keV x-rays. The ratio of the XDA to BND detector is plotted vs. the horizontal (Y-axis) position of the XDA detector in the focal plane.

An example of the expected shape of the X-ray spectrum incident on the BND and VETA is shown in Figure 6. For this molybdenum target, the continuous histogram shows the bremsstrahlung continuum extending up to 17 keV, corresponding to the setting of the generator high voltage. The notch above 2.3 keV is due to using a Mo filter to reduce this continuum. Mo has a complex of L-shell lines around 2.3 keV, with the five strongest spread over the region 2 to 2.5 keV. In all our fitting, we treat the multiple K or L shell lines with fixed ratios as tabulated in Salem et al. 1974, and treat the total line flux resulting in the fits as being at the weighted mean energy. The bremsstrahlung continuum shape is taken to be the thick target result, $\frac{dn}{dE}\alpha(E_{max}-E)/E$, where $n$ is the number of bremsstrahlung x-rays at energy $E$, and $E_{max}$ is the electron acceleration voltage.

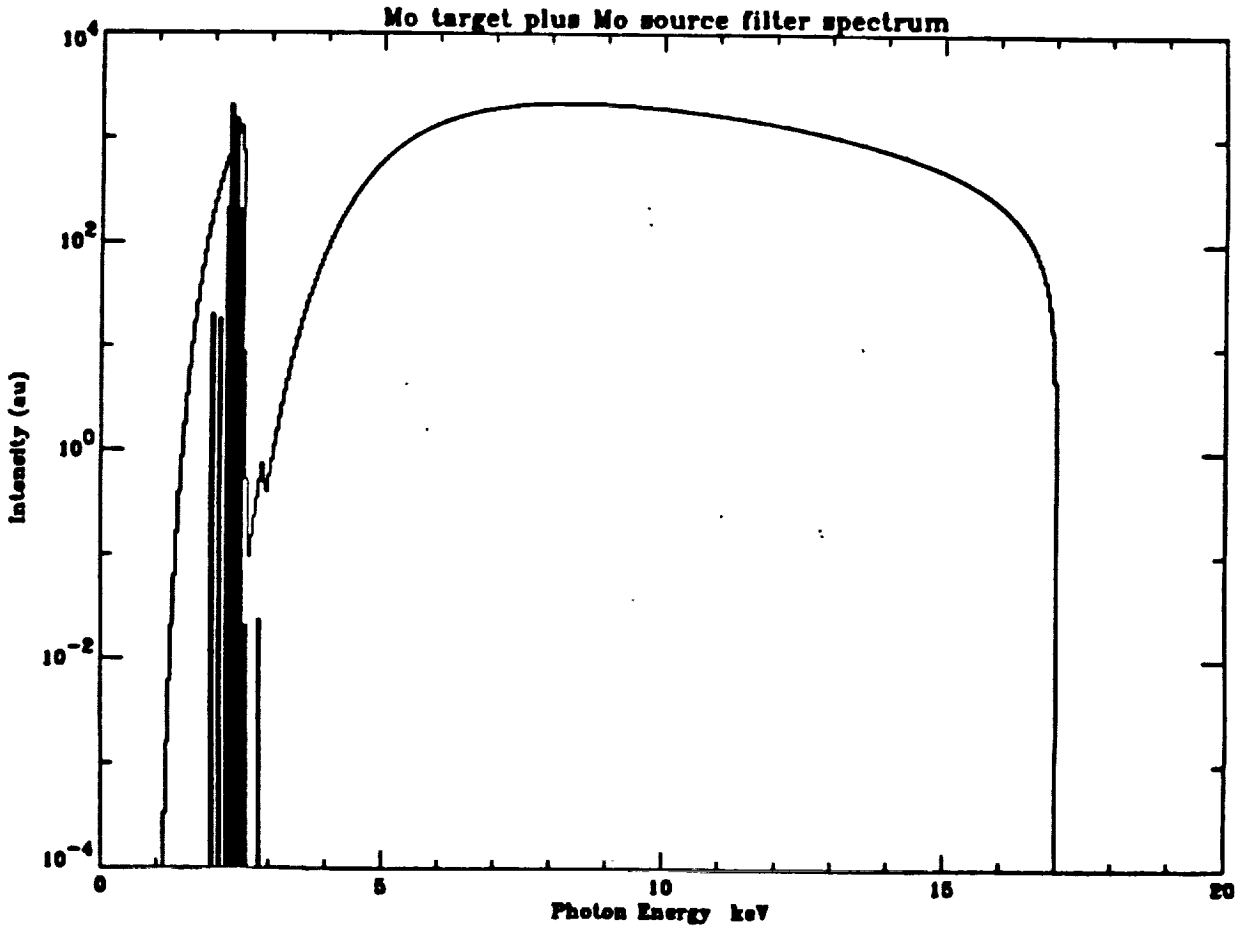


Figure 6. Deduced shape of the spectrum from the molybdenum target, incident on the BND detector. We see the bremsstrahlung continuum, and the complex of L-shell lines centered on 2.33 keV. The intensity is in arbitrary units, plotted in 50 eV wide bins.

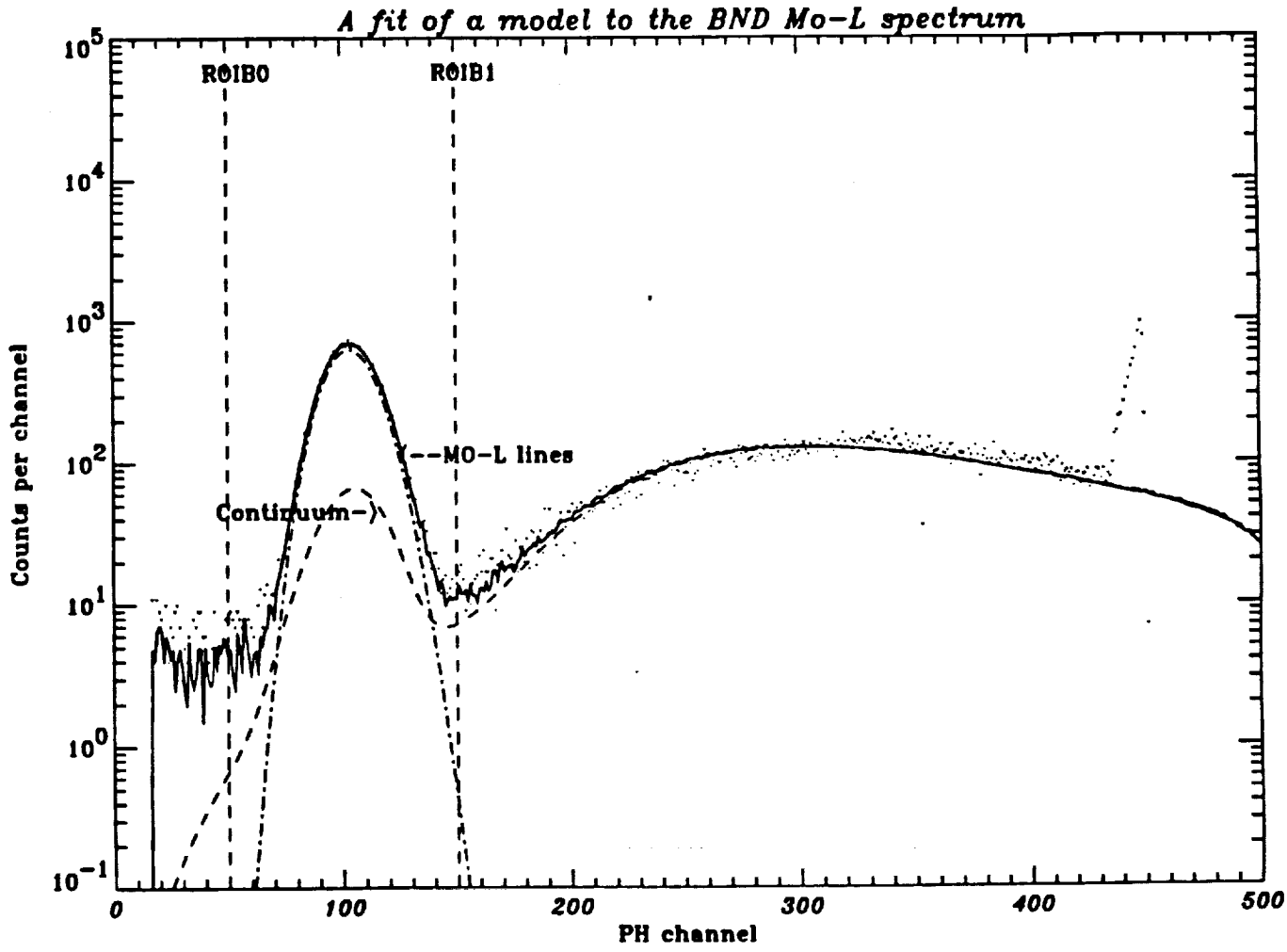


Figure 7. Response of the BND pulse height analysis, dots, compared with that expected by fitting the counter response to the input model of figure 6. The peak at channel ~100 is the response to all the L-shell lines, smeared out by the detector resolution. The lower solid line is the fit to the bremsstrahlung continuum, and the upper continuous line is the sum of the line and continuum component. The data analysis depends on the fit within the pair of vertical dashed lines designated ROIB0 and ROIB1 (see Chartas et al., 1992). (The measured counts pile up around our upper threshold, at about channel 450.)

Figure 7 is a typical pulse height spectrum observed in the BND for Mo X-rays. The key feature of the proportional counter response is that its modest energy resolution greatly broadens and blends all the X-ray lines, and also smooths out the sharp features due to the filter. In our data analysis, we subtract non-X-ray background, and perform fits to determine the strength of the lines, the continuum normalization, the energy resolution parameter using a Prescott response function, and the peak channel of the X-ray lines. As discussed by Chartas et al. (1992), we take the actual counts in the region of interest, shown as the vertical dashed lines, and subtract the number of counts determined by the fit to the bremsstrahlung continuum.

Figure 8 shows the analysis of the precision of extracting the X-ray line counts from the BND according to the process just described. The number of total counts in the region of interest is typically a few thousand to less than 100,000, so we show a 0.4 to 1.5 percent error in the statistics of the line peak counts. Generally, the X-ray generator flux is observed to be stable in time over a few minutes to a few hours, so we average from 2 to 20 different BND spectra in order to obtain one single fit with which to compare a series of focal plane measurements. This reduces the net error to the 0.1 to 1% range.

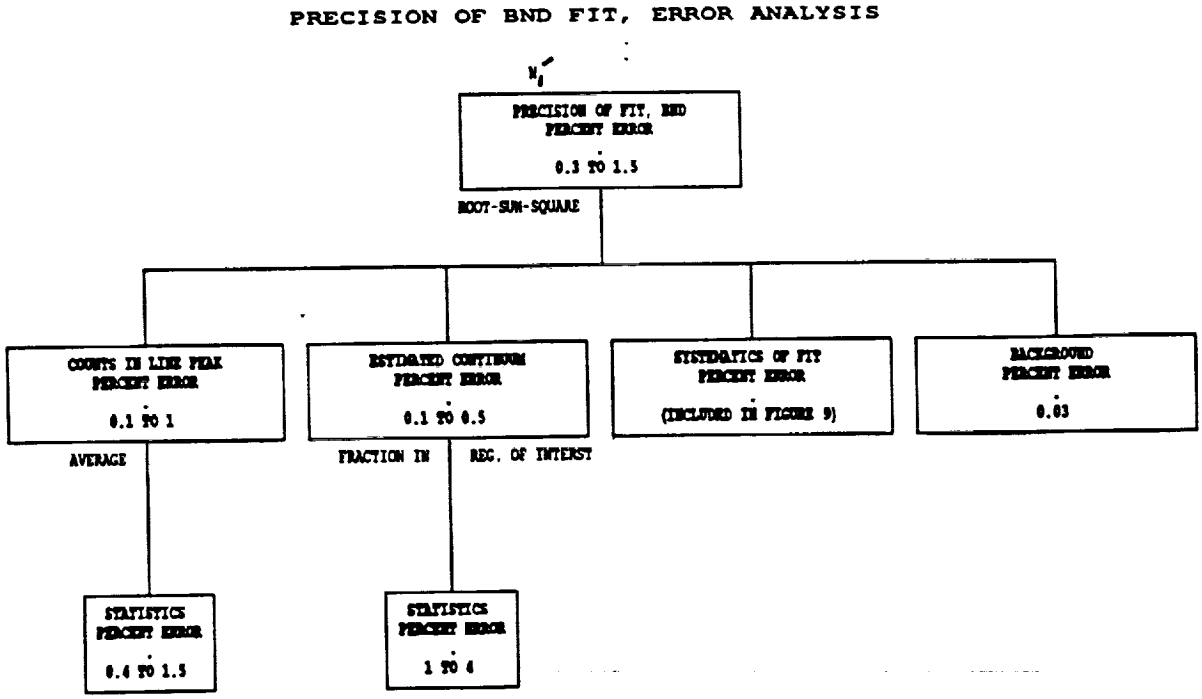


Figure 8. Analysis of the uncertainty in $N_1'$, the fit to the number of counts from the X-ray line as measured in the BND detector. The error is dominated by the Poisson fluctuations in the number of counts in the line peak and in the continuum. The systematic errors of the fit are all attributed to the XDA counts, since it is only errors in the ratio of XDA to BND which affect the encircled energy results.

The number of counts inferred as the continuum contribution ranges from ~600 to 10,000, so its flux is approximately determined to 1 to 4% of its own value. When averaged, and expressed as a fraction of the line flux, the estimated error ranges from 0.1 to 0.5%.

In the figure, we include a term to allow for errors which result from the systematics of the least-squares-fit process. These arise due to parameters which are kept fixed, e.g., the X-ray generator high voltage or the proportional counter window thickness, for which the value assumed may be incorrect. For analysis purposes we will assess all these effects when we consider the focal plane detector errors, since it is only the error in the ratio of counts that affects encircled energy.

We measure non-X-ray background when the gate valve to the X-ray generator is closed. We typically integrate long enough to acquire 1000 counts, so that the background flux is known to ~3%. The BND counting rates are always 100 times higher than background, so that this gives only 0.03% effect on the fitted counts.

We assume all other effects are each less than 0.1%, and we do not discuss them further since they contribute negligibly to the root-sum-square error. An example is the exact choice of the "region of interest" boundaries, as shown by Chartas et al. 1992 (their Figure 9).

4.3 Error Analysis of the Focal Plane Detector Counts.

Figure 9 presents the top level analysis of the focal plane detector counts. The relative live time box is repeated here for completeness, but has zero entry since we formally included its effects in the BND rate.

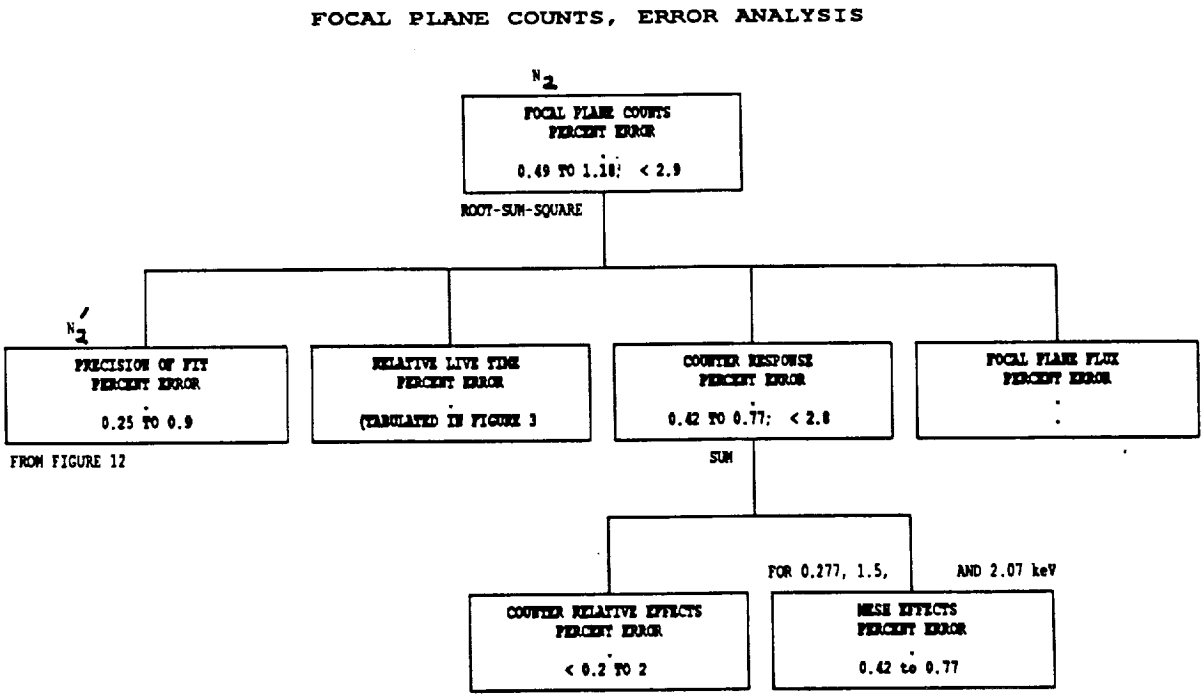


Figure 9. The error analysis for $N_2$, the idealized number of counts in the focal plane detector. PRECISION OF FIT error is shown in figure 12. The FOCAL PLANE FLUX error term would enter in the discussion of the true absolute effective area, but is shown blank here. MESH EFFECTS are discussed in Zhao et al. (1992).

The "counter response" term is intended to include intrinsic differences in the focal plane detector relative to the BND detector, (omitting terms due to "systematics of fit" discussed in figure 12). The primary effect is due to the window support mesh, as discussed in detail by Zhao et al. (1992). For the C-K (0.277 keV), Al-K (1.49 keV), and Zr-L (2.07 keV) lines the estimated residual uncertainty after performing the correction is 0.5%. For the Cu-L (0.93 keV), and Mo-L (2.3 keV) lines we did not scan the counter windows behind the pinholes as is necessary to perform the correction. In this case we assume the ±8% full range of the possible correction is a uniform distribution (for which the rms is $1/\sqrt{12}$), and therefore take $16\%/\sqrt{12} = 4.4\%$ as the error.

The term "counter relative effects" is intended to account for unexpected ways in which the BND and focal plane detectors differed. (Expected possible differences are analyzed in the "systematics of fit" term in figure 12.) It was planned that we would correct for these unexpected differences by simply swapping the positions of the two counters and comparing the ratios of counts in the swapped vs. normal positions. Unfortunately, the window on the BND

counter was broken before this swap could be performed. The transparency of the actual window is an important determinant of the proportional counter response, so it is not valid to perform the swap with a replaced window and use it to correct the VETA data. Instead, we studied the ratios with the counters swapped for the replaced window, and interpret the apparent difference as an upper limit to the error. In the case of Al-K X-rays the two ratios, for the raw counting rate data, were 1.037 and 1.039, while for Cu-L X- rays the ratios were 1.063 and 1.042. We thus show 0.2 to 2 percent as a upper limit to this error term. We treat the actual error as zero. From this data, we estimate that for the flight mirror we will be able to perform this correction to within a residual 0.2% error.

In figure 10 we show the estimated X-ray generator spectrum from the Al target. We see the Al-K lines (solid), and the bremsstrahlung continuum (dotted) modified by the Al filter. The dot-dash line indicates the expected spectral shape incident on the focal plane. Because the VETA mirror response cuts off sharply above 2 keV, the continuum spectrum is significantly modified. Figure 11 shows the pulse height spectrum as recorded in the focal plane proportional counter. We notice the continuum contribution is reduced, relative to the BND spectra. We also see a broad peak at about twice the Al-K energy. This is due to pile up of Al-K X-rays, since we are typically counting at several thousand per second. Although prominent on the graph, it is less than 1% of the Al line counts, and it is known to within a few percent of its own estimated value (from figure 5 of Chartas et al. 1992), so that it gives less than a few hundredths percent error to the focal plane counts.

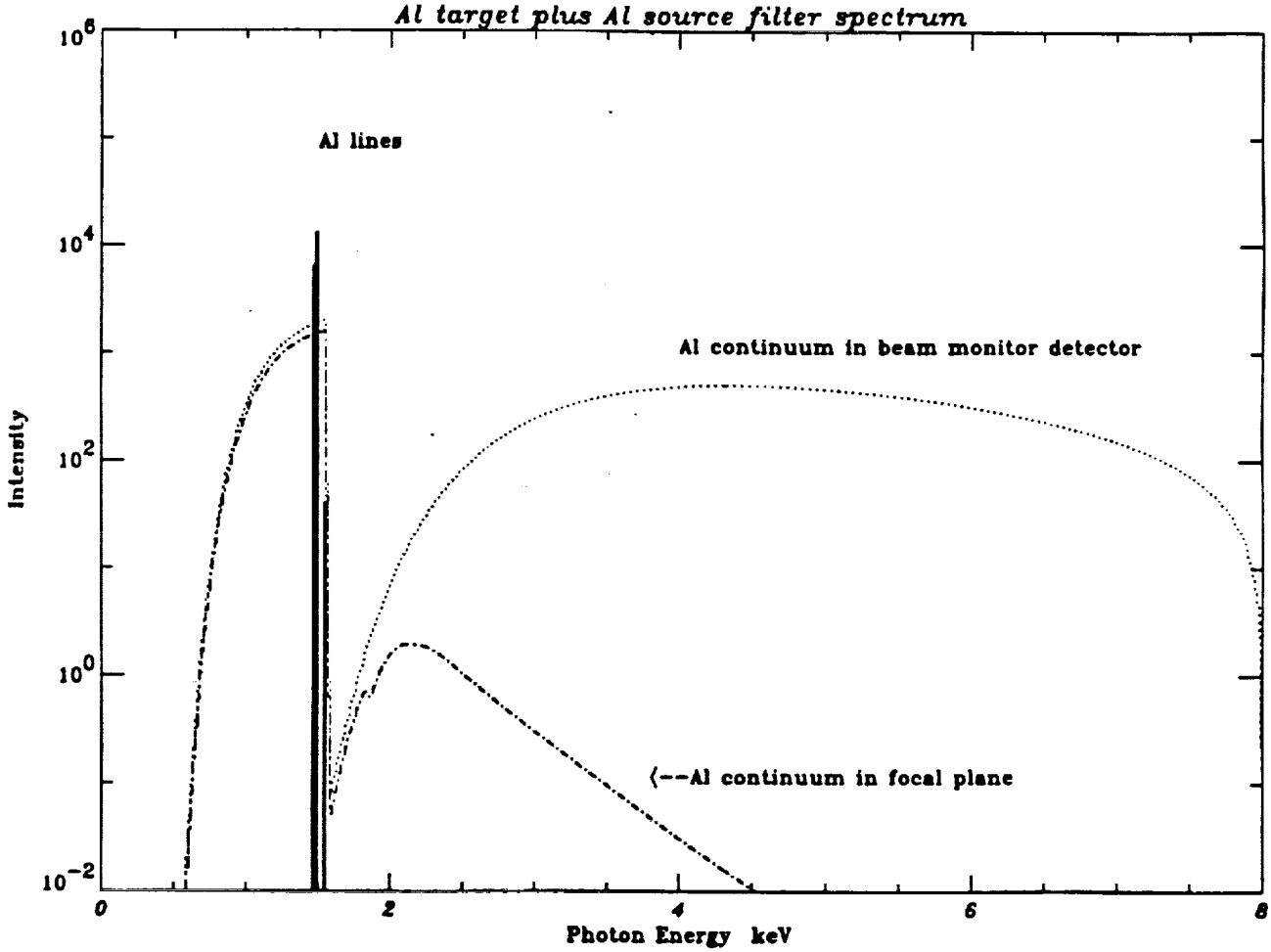


Figure 10. Deduced shape of the spectrum from the aluminum target, as incident on the VETA (dotted line) and incident on the XDA detector after reflection by the mirror (dash-dot line). We see the bremsstrahlung continuum, and the K-shell lines centered on 1.49 keV. The intensity is in arbitrary units.

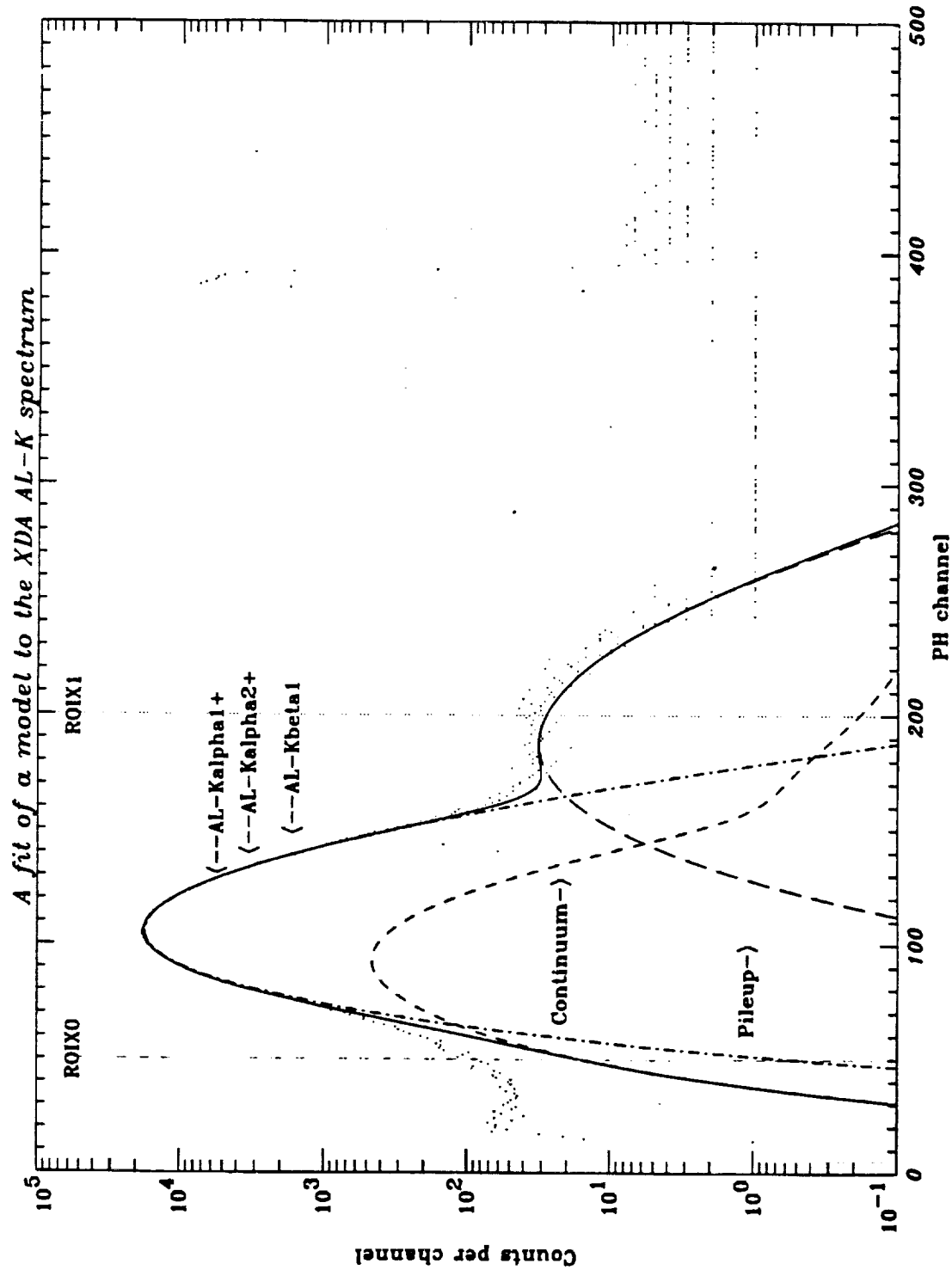


Figure 11. Response of the XDA pulse height analysis, dots, compared with that expected by fitting the counter response to the input model of figure 10. The peak at channel ~100 is the response to the K-shell lines, smeared out by the detector resolution. The peak at channel ~200 is from pulse pile-up. The short dashed line is the fit to the bremsstrahlung continuum, and the upper solid line is the sum all components. The data analysis depends on the fit within the pair of vertical dashed lines designated ROIX0 and ROIX1 (see Chartas et al., 1992). (The pulser used for dead time estimation peaks at about channel 390.)

Figure 12 analyzes the precision of fitting to the line counts in the focal plane detector. The data analysis proceeds by taking all the measured counts within the region of interest indicated by the vertical lines, subtracting the fit to the continuum, subtracting that part of the fit to the pile up peak which falls within the region of interest, and adding twice the total number of counts fit to the entire pile up peak, since these pile up events are each two 1.49 keV X-rays.

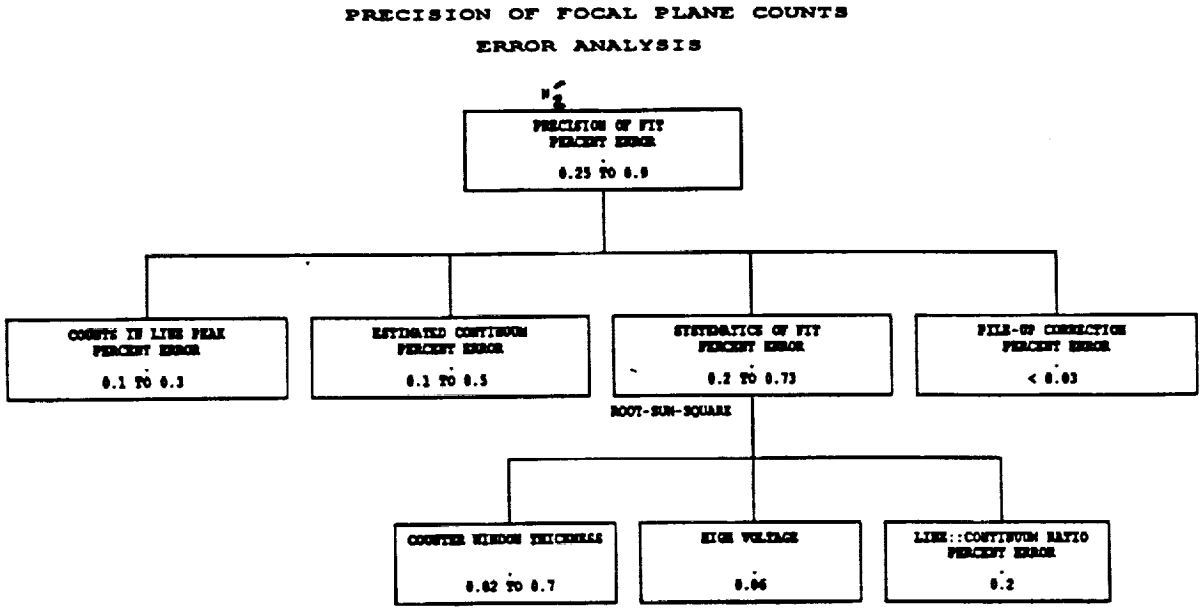


Figure 12. Error analysis for $N_2'$, the fit to the number of counts in the X-ray line. The COUNTS IN LINE PEAK and ESTIMATED CONTINUUM boxes are the Poisson statistical errors. See text for SYSTEMATICS OF FIT errors.

Counts in the line peak are typically $10^5$ to $10^6$, giving a 0.1 to 0.3 percent error. The pile-up correction itself is about 1 to 3%, known to an accuracy of about 1%. The background is known to about 3%, but is less than 0.001 of the line counts. The significant new term in this error tree is that due to the systematics of the fit. The three dominant terms are due to the counter window thickness, the ratio of the line to continuum counts in the incident X-ray spectrum, and the high voltage setting of the X-ray generator. Each of these is held as a fixed, given parameter during the fit to determine the number of counts in the X-ray line.

We perform a sensitivity analysis to assess the effects of those terms. Figure 13 shows the effect of varying the proportional counter window thickness from its nominal value of $1.7 \pm 0.2$ microns. The top panel for each energy (13a for 1.49 keV, 13b for 0.277 keV), shows how the number of fitted counts changes as a function of fixing different window thickness parameters. The bottom panel shows the percentage error. The effect is greatest at the lowest energy, C-K where the window is most opaque.

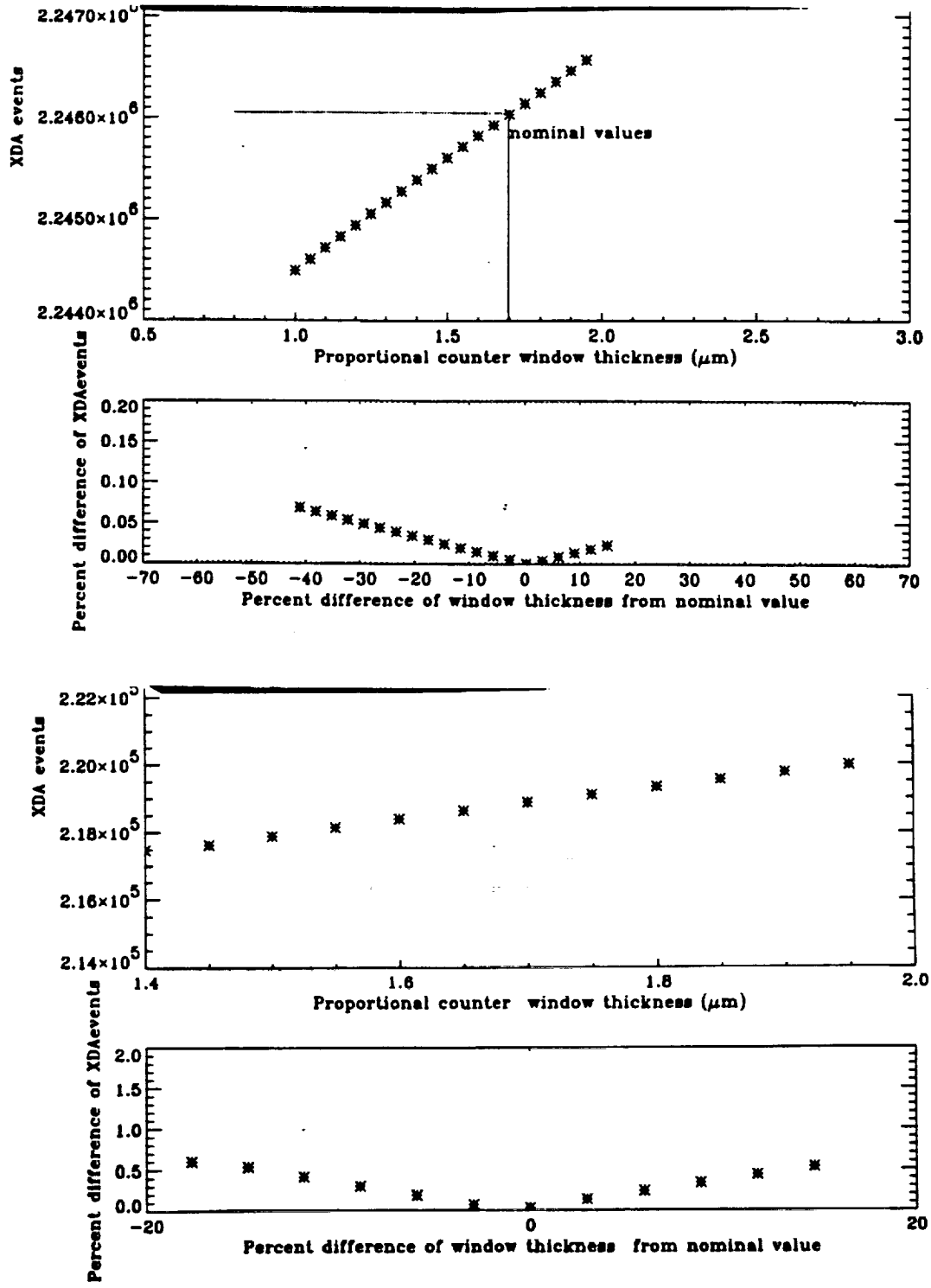


Figure 13. Systematic change of the deduced line counts for Al-K X-rays (fig. 13a, upper 2 graphs) and for C-K X-rays (fig. 13b, lower 2 graphs), vs. the true proportional counter window thickness. The bottom panels of 13a and 13b show the percentage change in deduced line counts vs. the percentage change in window thickness. The nominal error in knowledge of the window thickness is 0.2 microns.

Figure 14 shows the effect of varying the assumed value of the high voltage setting of the X-ray generator, on the fitted counts from Al. Within the assumed 1% tolerance on the generator setting, the deduced counts change by less than 0.06%.

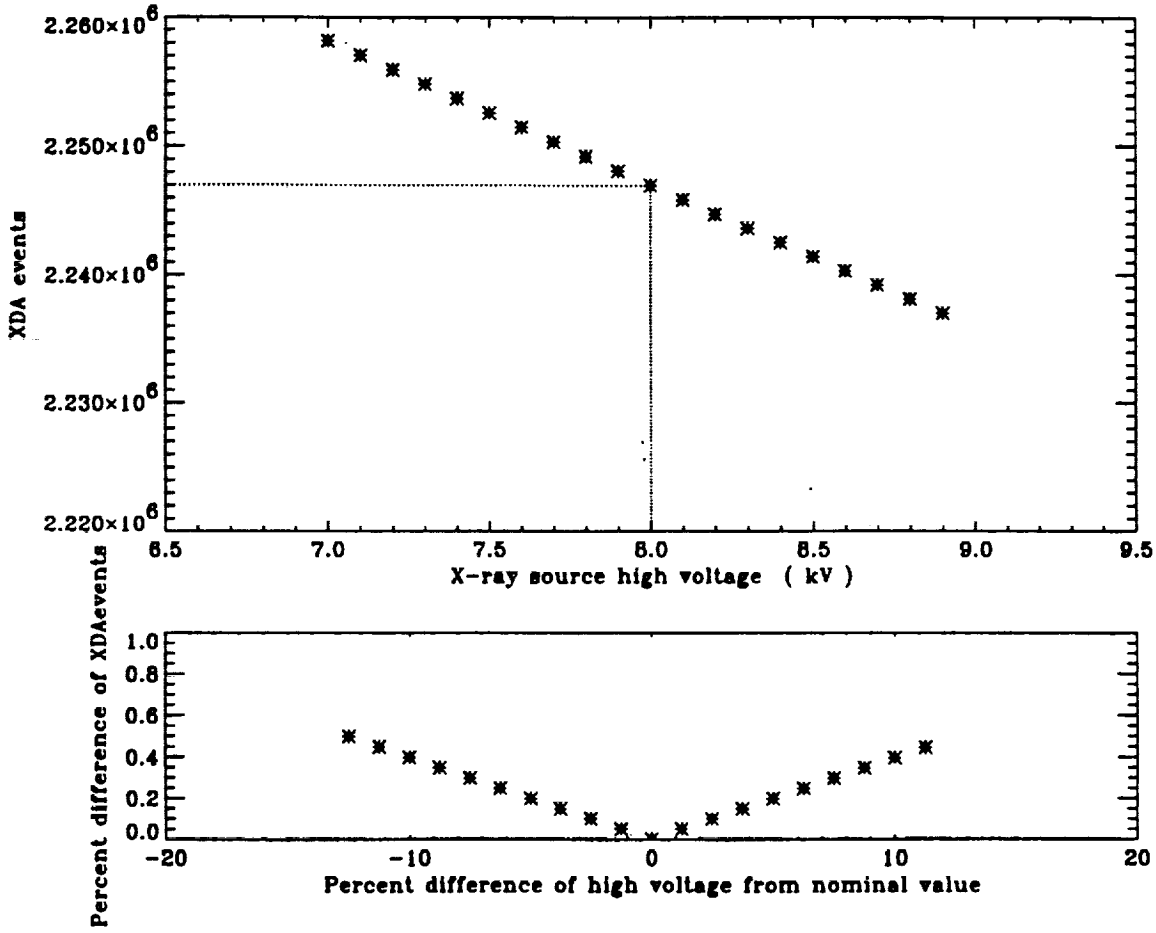


Figure 14. Systematic change of the deduced line counts for Al-K X-rays vs. the true high voltage setting of the X-ray generator. The assumed accuracy of the high voltage setting is 1%.

In fitting the focal plane counts, we assume that the incident X-ray line to bremsstrahlung continuum ratio is the same as determined from the fit to the BND data, and modified subsequently by the mirror reflectivity. Figure 15 shows how the line strength and continuum strength parameters are independently fitted to the BND data. The range of variation of the ratio is taken from the extremes on the 95% confidence contour, and applied in figure 16 to the analysis of the sensitivity of the Al counts, resulting in a 0.2% error.

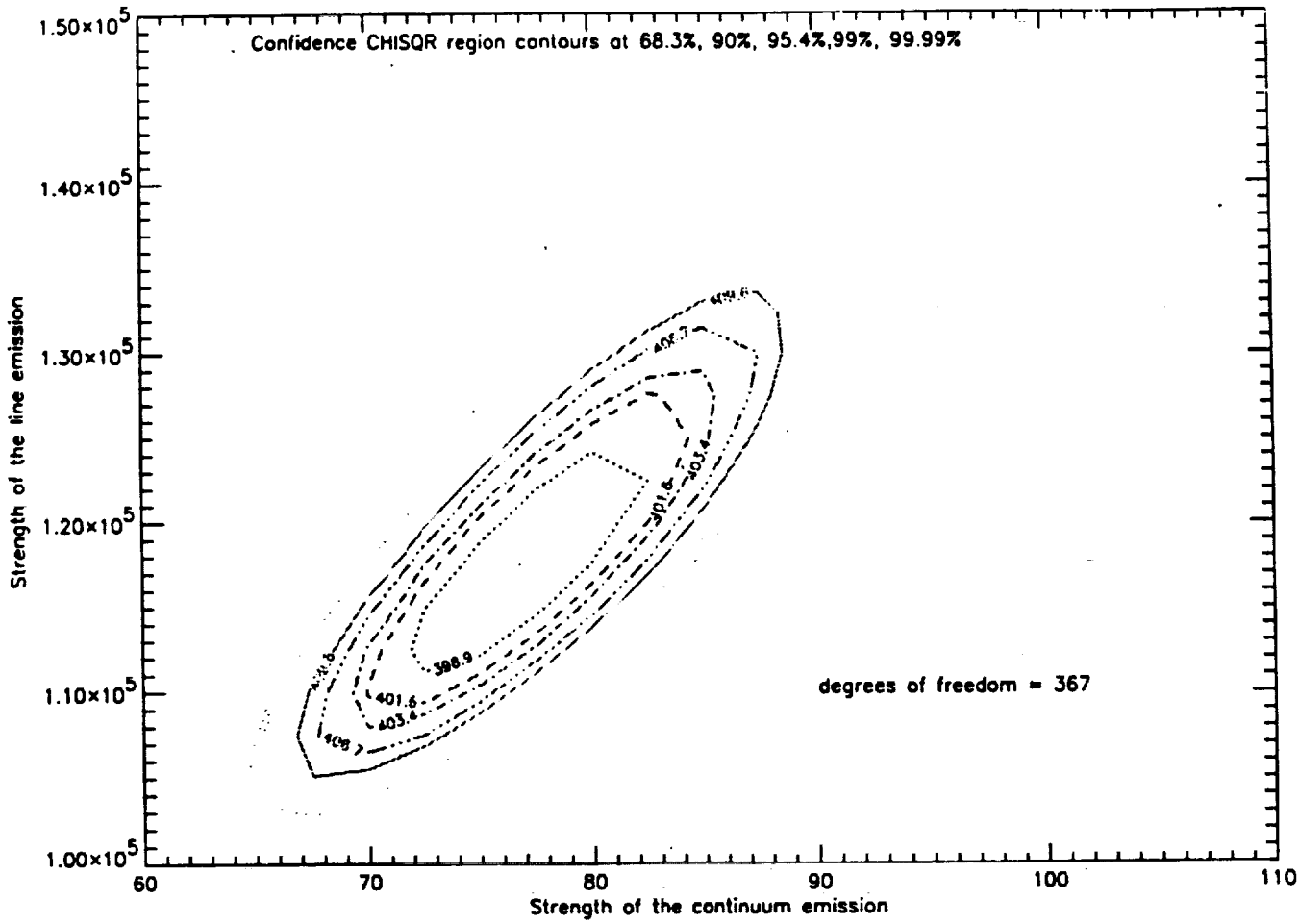


Figure 15. Chi-squared contours for jointly determining the line strength and the continuum strength from the BND data for the Al target. We take the extreme range of variation of the ratio of line to continuum flux (about 5%), along the 95% confidence contour, to estimate the uncertainty of the focal plane counts due to this systematic error.

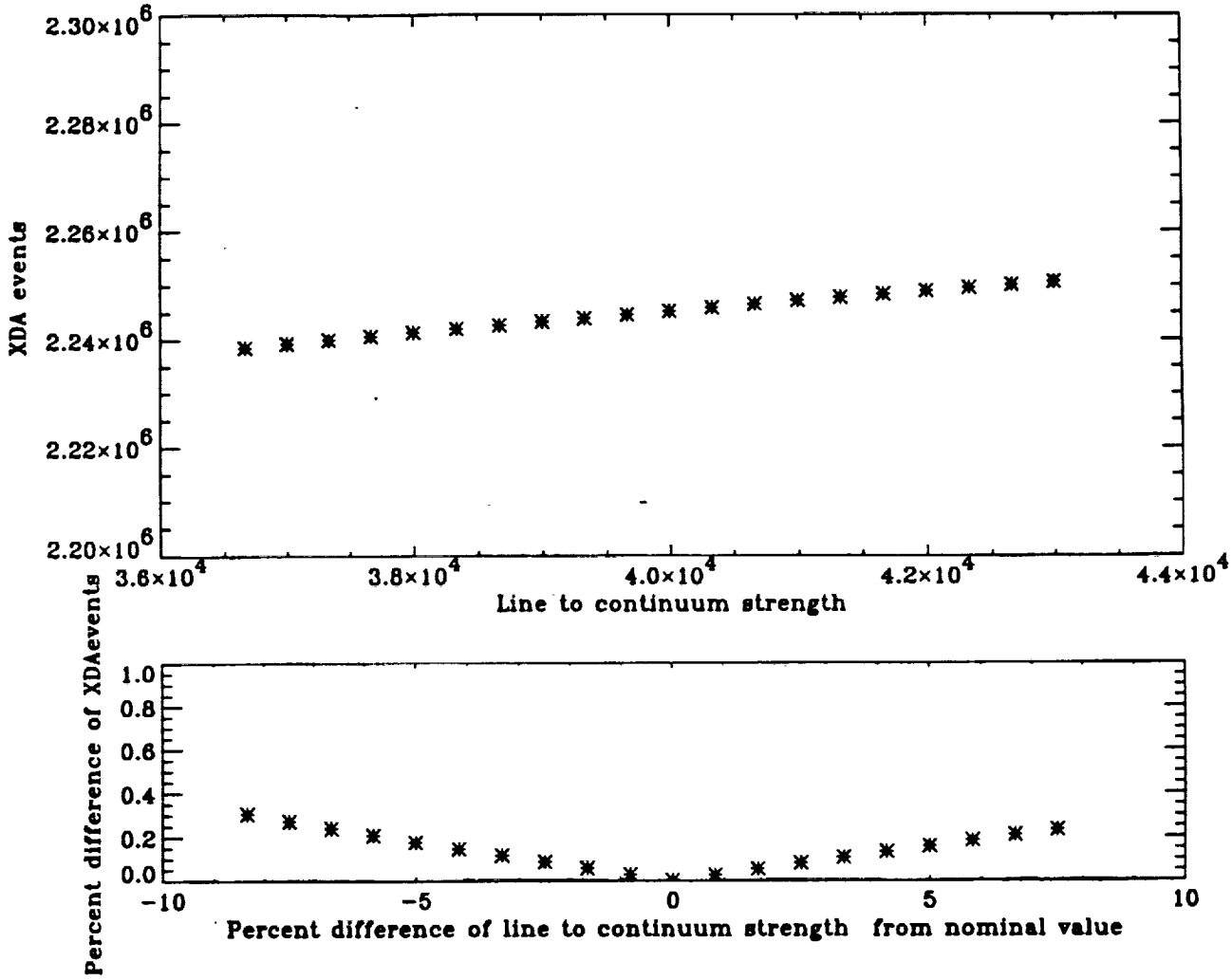


Figure 16. The upper panel shows the systematic change of the deduced line counts for Al-K X-rays vs. the true value of the line to continuum strength (plotted in arbitrary units). The lower panel shows the percentage error in Al line counts vs. the assumed percentage error in the ratio. The nominal error in the ratio is ~5%, to 95% confidence.

## 4.4 Summary

Figure 17 summarizes the error estimates for the 3 most reliable energies, and for pinholes of diameter 3 arcsec and larger. The proportional counters could not be centered at the same precise position behind the pinholes of radius 20 and 100 arcsec as for the other pinholes, and this may be reflected in a slightly larger error for some of those data points. Within the internal accuracy of the estimates of the error of each point, the errors are probably consistent with the mean for all pinhole sizes of each given energy: 1.07% for 0.277 keV, 0.75% for 1.49 keV, and 0.89% for 2.07 keV. It is reasonable that the errors would be the same, since this range of pinhole radii all contain greater than 80% of the encircled energy.

# ENCIRCLED ENERGY ERROR

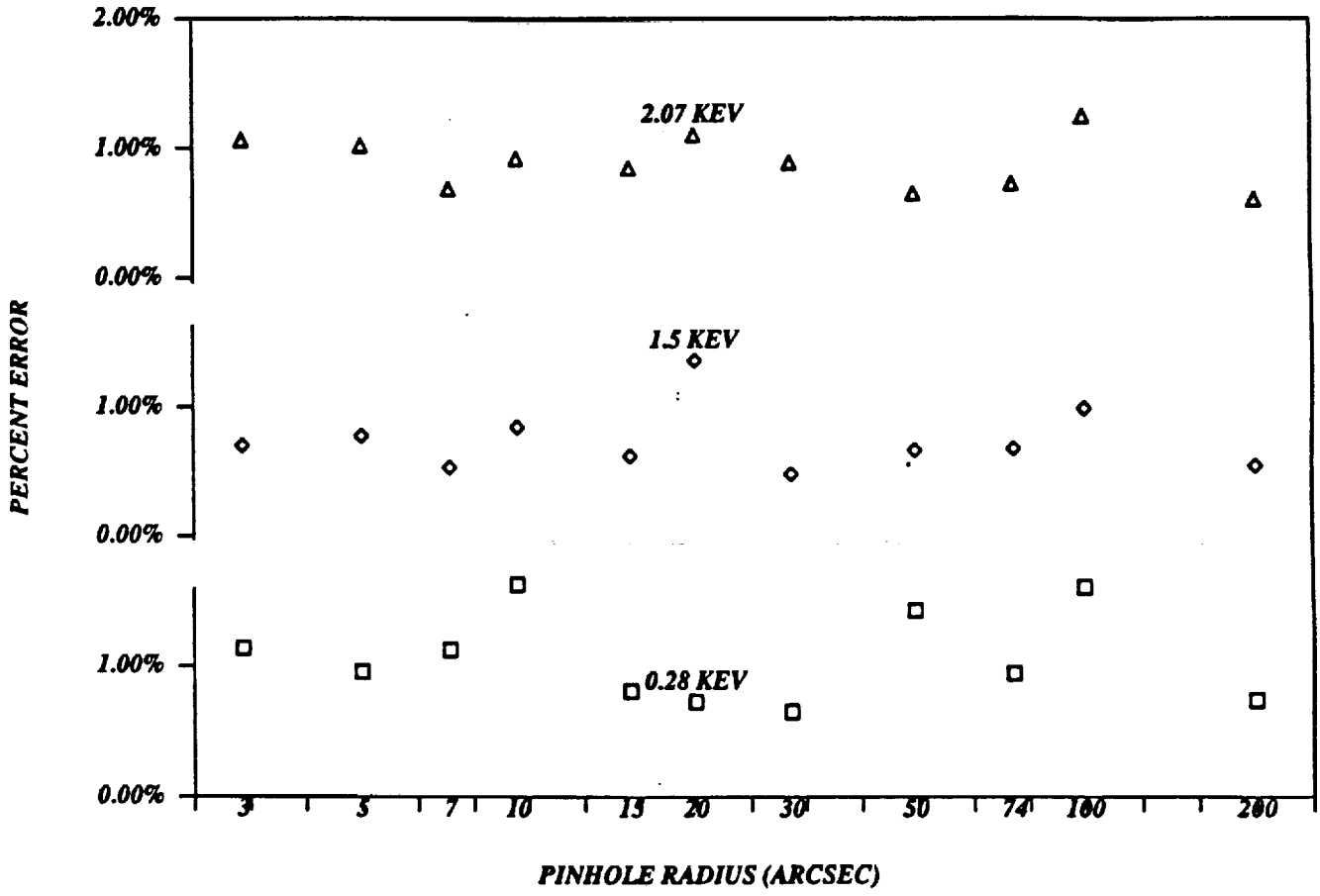


Figure 17. Percentage error on the Encircled Energy Area, for pinholes of radius 3 arcsec and larger, at the C-K, Al-K, and Zr-L X-ray lines. The scatter for the different size pinholes is consistent with a constant error of 1.07% at 0.277 keV, 0.75% at 1.5 keV, and 0.89% at 2.07 keV.

Assuming the error for each energy is constant, independent of pinhole size, we use the rms scatter of the 11 data points to calculate the precision to which we have estimated the mean error at each energy. We find 0.35% for 0.277 keV, 0.24% for 1.49 keV, and 0.20% for 2.07 keV, as the uncertainty in how well we know the errors at those energies. This justifies quantitatively our ignoring some of the errors of magnitude less than 0.1%.

The precision of making VETA measurements makes us optimistic that we can achieve our goal of predicting the on-orbit AXAF telescope performance to a precision of order 1%. The correction of ground calibration data to on-orbit prediction also depends on the accuracy of the models of how the telescope will distort in the presence of gravity. This uncertainty is expected to be of order 1% itself, therefore we desire to improve the ground measurements by another factor of ~2, but will encounter diminishing returns for further improvement beyond that point. Understanding the counter effects of window thickness and mesh shadowing, and obtaining increased characterization of the X-ray spectrum produced by the generator, offer significant error reduction. In addition, we know that for the VETA test we were subject to systematic errors due to X-ray beam spatial irregularities and systematic counter differences. Direct measurement and correction for these effects is planned for the AXAF flight mirror calibration.

## 5. ACKNOWLEDGMENTS

We thank M. Birkinshaw and H. Tananbaum for comments on the manuscript. R.Brissenden, J. Chappell, M. Freeman, D. Graessle, M. Jones, M. Joy, J. Kolodziejcak, D. Nguyen, T. Norton, W. Podgorski, J. Roll, P. Slane and L VanSpeybroeck all played important roles in carrying out the VETA-I tests and analyses. We thank many MSFC, TRW, and EKC personnel for heroic efforts in preparing facilities and supporting the execution of the test. This research was supported in part by NASA contract NAS8-36123.

## 6. REFERENCES

Brissenden, R.J.V., Hughes, J.P., Kellogg, E.M. and Zhao, P., Internal SAO report SAO-AXAF-AR-91-080, 15 November 1991.

Brissenden, R.J.V., Chaartas, G., Hughes, J.P., Kellogg, E.M. and Zhao, P., Internal SAO report SAO-AXAF-AR-92-002, 10 January 1992.

Chartas, G., Flanagan, K.A., Hughes, J.P., Kellogg, E.M., Nguyen, D., Zombeck, M., Joy, M., and Kolodziejcak, J. 1992, *SPIE Proceedings*, **1742**, (this volume).

Hughes, J.P., Schwartz, D.A., Szentgyorgyi, A., VanSpeybroeck, L., and Zhao, P. 1992, *SPIE Proceedings*, **1742**, (this volume).

Kellogg, E.M., Chartas, G., Graessle, D., Hughes, J.P., VanSpeybroeck, L., Zhao, P. Weisskopf, M.C., Elsner, R.F., and O'Dell, S.L., 1992, *SPIE Proceedings*, **1742**, (this volume).

Kellogg, E.M., Brissenden, R.J.V., Flanagan, K.A., Freeman, M., Hughes, J.P., Jones, M., Ljungberg, M., McKinnon, P., Podgorski, W., Schwartz, D.A., Zombeck, M., 1991a, *SPIE Proceedings*, **1546**, 2.

Kellogg, E.M., et al. 1991b, [abstract], *B.A.A.S.*, **23**, 1349.

Podgorski, W.A., Flanagan, K.A., Freeman, M.D., Goddard, R.G., Kellogg, E.M., Norton, T.J., Ouellette, J.P., Roy, A.G., and Schwartz, D.A., 1992, *SPIE Proceedings*, **1742**, (this volume).

Salem, S.I., Panossian, S.L., and Krause, R.A. 1974, *Atomic and Nuclear Data Tables*, **14**.
Schwartz, D.A., McKinnon, P.J., Murray, S.S., Primini, F.A., VanSpeybroeck, L.P., Zombeck, M.V., Dailey, C.C., Reily, J.C., and Weisskopf, M.C. 1986, *SPIE Proceedings*, J.L. Culhane, ed., **587**, 10.

VanSpeybroeck, L.P., McKinnon, P.J., Murray, S.S., Primini, F.A., Schwartz, D.A., Zombeck, M.V., Dailey, C.C., Reily, J.C., Weisskopf, M.C., Wyman, C.L., Glenn, P., and Slomba, A. 1986, *SPIE Proceedings*, J.L. Culhane, ed., **597**, 20.

VanSpeybroeck, L.P., Reid, P., Schwartz, D.A., and Bilbro, J., *SPIE Proceedings*, **1160**, 94.

Wyman, C.L., Dailey, C.C., Reily, C., Weisskopf, M., McKinnon, P.J., Schwartz, D.A., and VanSpeybroeck, L.P., 1986, *SPIE Proceedings*, J.L. Culhane, ed., **597**, 2.

Zhao, P., Freeman, M.D., Hughes, J.P., Kellogg, E.M., Nguyen, D.T., Joy, M., and Kolodziejczak, J.J. 1992b, *SPIE Proceedings*, **1742**, (this volume).

Zhao, P., Kellogg, E.M., Schwartz, D.A., Shao, Y., and Fulton, M.A. 1992a, *SPIE Proceedings*, **1742**, (this volume).